Available online at www.sciencedirect.com
SCIENCE DIRECT®
PERGAMON
International Journal of Heat and Mass Transfer 46 (2003) 2655–2663
International Journal of HEAT and MASS TRANSFER
www.elsevier.com/locate/ijhmt

Numerical study for enhancement of laminar flow mixing using multiple confined jets in a micro-can combustor

Peter L. Woodfield [a,1], Kazuyoshi Nakabe [b,2], Kenjiro Suzuki [a,*]

[a] *Heat Transfer Laboratory, Department of Mechanical Engineering, Kyoto University, 4-6-1 Komaba, Meguro-ku, Kyoto 606-8501, Japan*

[b] *Applied Energy Science Laboratory, Department of Energy System Engineering, Osaka Prefecture University, Sakai, Osaka 599-8531, Japan*

Received 27 September 2002; received in revised form 28 November 2002

Abstract

To meet demands arising as a result of present trends towards miniaturization, an innovative design for promoting mixing enhancement in a miniature can combustor is investigated using an unstructured finite-volume technique. A multi-holed baffle plate is employed to create a ring of oxidizer jets surrounding a single fuel jet in parallel with the axis of the cylindrical chamber. The baffle plate is found to produce a dramatic improvement to the mixing performance when compared with simpler co-axial jet cases. Relatively small changes in geometry are found to have a major influence on mixing for laminar isothermal flow.

1. Introduction

As a result of the present global trend towards miniaturization, increasingly more attention is being given to the behavior of flows at low Reynolds number [1–5]. For mini-scaled combustion systems one of the key issues is the mixing of fuel and oxidizer streams or the mixing of incoming reactants with high temperature gases resident in the combustor. To realize a practical device for this situation, it is necessary to find a method for enhancing mixing within miniature chambers.

The challenge to rapidly mix or entrain fluids at low Reynolds number has been a source of innovation in the open literature. It has been shown that crossing two laminar jets at a small angle can aid mixing by invoking a transition to turbulent flow and can hence improve the performance of a miniature jet pump [6]. Directly opposed jets have been proposed for small combustors and in the design of low Reynolds number mixers for reaction injection molding (RIM) [7,8]. Acoustic excitation of jets at low Reynolds number [6] offers another relatively unexplored means of achieving higher mixing rates by inducing an early transition to turbulent flow. In the present study a new solution to this problem is presented whereby convective mixing enhancement is achieved through the introduction of a multi-holed baffle plate in a cylindrical can combustor as shown in Fig. 1.

The present investigation is a part of a much larger project to develop a combustor for a micro-gas turbine (MGT) to be used within a distributed hybrid solid oxide fuel-cell/MGT energy generation system [1]. Although the authors primarily are interested in the performance of the above design for turbulent flow at low *Re*, this paper focuses on the laminar regime which may be applicable during the start-up phase of the system and for applications where size limitations necessitate laminar flow (for example Ref. [2]). In addition, the laminar study provides valuable insight into the convective mixing process associated with this design without the additional complication due to turbulence. The present work extends the previous work of the authors

* Corresponding author. Tel.: +81-75-753-5250; fax: +81-75-753-5851.

E-mail addresses: peter@htlab.mbox.media.kyoto-u.ac.jp (P.L. Woodfield), nakabe@energy.osakafu-u.ac.jp (K. Nakabe), ksuzuki@mech.kyoto-u.ac.jp (K. Suzuki).

[1] Tel.: +81-75-753-5218; fax: +81-75-753-5251.

[2] Tel.: +81-72-254-9224 (off.); fax: +81-72-254-9905 (admin. off.).

0017-9310/03/$ - see front matter © 2003 Elsevier Science Ltd. All rights reserved.
doi:10.1016/S0017-9310(03)00014-0

Nomenclature

$b_{(\phi)}$	source term
B_i	'i'th component of unit vector in direction I–J in Fig. 2
c	mid-point of line I–J
D	diameter
Nu	Nusselt number
p	pressure
Re	Reynolds number, $\rho UD/\mu$
$\vec{S}_{(c)}$	vector representing all facets of the control volume connected to point 'c'
S_i	'i'th component of the vector $S_{(C)}$
U	mean velocity over cross-section
u_i	'i'th component of velocity
x_i	Cartesian coordinate
X	locally rotated Cartesian coordinate aligned with edge direction
x	Cartesian coordinate ($=x_1$)
y	Cartesian coordinate ($=x_2$)
z	Cartesian coordinate ($=x_3$)

Greek symbols

Γ	diffusion coefficient
$\Delta_{(IJ)}$	distance from point 'I' to point 'J'
μ	dynamic viscosity
ξ	mixture fraction
ρ	density
σ	Schmidt number
ϕ	dependent variable

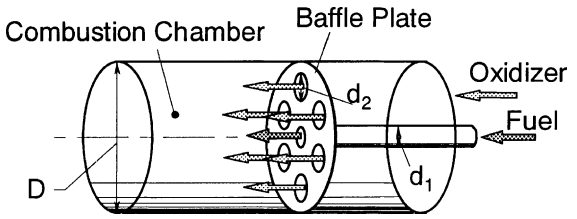

Fig. 1. Chosen design for investigation.

[3] to include the region upstream of the baffle plate within the calculation domain and to investigate more thoroughly the mixing performance of the device for a wider range of possible configurations of the holes.

In order to separate the effects of chemical reaction from those of convective mixing, but yet include the mixing of two different chemical species, fuel and oxidizer, the flow investigated is taken to be non-reacting, isothermal and of constant density. This allows the energy equation to be decoupled from the system. Although only constant property cases are considered in the present work, the mathematical and numerical formulations allow for straight forward extension to variable property problems.

2. Mathematical model

2.1. Governing equations

Eqs. (1) and (2) show unsteady mass and momentum conservation equations for incompressible flow.

$$\frac{\partial(\rho u_j)}{\partial x_j} = 0 \tag{1}$$

$$\frac{\partial(\rho u_i)}{\partial t} + \frac{\partial}{\partial x_j}(\rho u_j u_i) = -\frac{\partial p}{\partial x_i} + \frac{\partial}{\partial x_j}\left(\mu \frac{\partial u_i}{\partial x_j}\right) \tag{2}$$

Eq. (3) represents species conservation where ξ is the mass fraction of gas originating in the primary (fuel) stream and σ_ξ is the Schmidt number, here taken to be 0.7.

$$\frac{\partial(\rho \xi)}{\partial t} + \frac{\partial}{\partial x_j}(\rho u_j \xi) = \frac{\partial}{\partial x_j}\left[\frac{\mu}{\sigma_\xi}\frac{\partial \xi}{\partial x_j}\right] \tag{3}$$

2.2. Generalized form

Using the divergence theorem, Eqs. (2) and (3) can be expressed conveniently in integral form for an arbitrary control volume as given in Eq. (4).

$$\int\int\int_{\mathrm{Vol}} \left(\frac{\partial(\rho\phi)}{\partial t}\right) \mathrm{d}v + \int\int_{\mathrm{Surf}} (\rho u_j \phi n_j)\, \mathrm{d}s = \int\int_{\mathrm{Surf}} \left(\Gamma \frac{\partial \phi}{\partial x_j} n_j\right) \mathrm{d}s + \int\int\int_{\mathrm{Vol}} (b_{(\phi)})\, \mathrm{d}v \tag{4}$$

3. Numerical method

To accurately handle the complex geometry shown in Fig. 1, a vertex-centered unstructured finite-volume method is employed to discretize Eq. (4) over the computational domain. The computer code used in the simulation was written by the first author and full details of the method are given elsewhere [5]. For clarity of the discussion the main features of the code are summarized in the following.

3.1. Definition of control volume for integration

The computational domain is constructed entirely of hexahedrons with the unknowns being solved at the vertices. The median dual of the hexahedral mesh defines the control volumes surrounding each vertex as is shown for a typical case in Fig. 2.

The geometry shown in Fig. 2 is neatly summarized in the computer program as a set of three component vectors, assuming that the value of any variable or property interpolated to the mid-point of a line connecting the grid point 'I' to its neighbor 'J' is representative for all facets of the control volume which have a corner at 'c'. Only one vector, $\vec{S}_{(c)}$ is required for each 'edge' as is shown for edge I–J in Fig. 2. $\vec{S}_{(c)}$ equals the sum of the facet-area vectors for all facets of the control volume which have a corner at 'c' (where a 'facet-area vector' is defined as a vector normal to the facet having a magnitude equal to the area of the facet [5]).

3.2. Treatment of convection terms

The convection term in Eq. (4) is discretized as given in Eq. (5) where for the control volume surrounding a single point 'I', the summation includes all edges connecting 'I' to neighboring points 'J'.

$$\int\int_{\text{Surf}} \rho u_j \phi n_j \, \mathrm{d}s \approx \sum_{\text{NIneighbors}} \rho|_{\text{C}} \phi|_{\text{C}} \vec{u}|_{\text{C}} \cdot \vec{S}_{(\text{C})} \tag{5}$$

To determine $\phi|_{\text{C}}$ in Eq. (5) both the value of ϕ and its gradient at the upstream end of the line I–J are used in the interpolation. For example, if 'I' is the upwind point, $\phi|_{\text{C}}$ is given by Eq. (6) where uppercase 'X' denotes the direction I–J.

$$\phi|_{\text{C}} = \phi|_{\text{I}} + \frac{\Delta_{(\text{IJ})}}{2} \times \overline{\left(\frac{\partial \phi}{\partial X}\right)}\Bigg|_{\text{I}} \tag{6}$$

The gradient of ϕ at the grid point 'I' is approximated using a numerical discretization of the divergence theorem with a linear interpolation to the edge mid-point as given in Eq. (7).

$$\left.\frac{\partial \phi}{\partial x_i}\right|_{\text{I}} \approx \frac{1}{\text{Vol}_{(\text{I})}} \left(\sum_{\text{NIneighbors}} \frac{1}{2} (\phi|_{\text{I}} + \phi|_{\text{J}}) S_i|_{\text{C}} \right) \tag{7}$$

In this equation, '$S_i|_{\text{C}}$' is the 'i'th component of the vector, $\vec{S}_{(c)}$, shown in Fig. 2 and 'Vol$_{(\text{I})}$' is the volume of the control volume surrounding the point 'I'.

In order to prevent non-physical grid related overshoots appearing in the solution as a result of the second-order upwind interpolation, the criteria for preserving 'boundedness' given by Gaskell and Lau [9] are implemented in the same manner as the previous work of the authors [5]. Thus, to show that the slope has been controlled by a limiter an over-bar is included in Eq. (6).

The remaining parameter to be determined in Eq. (5) at 'c' is the volumetric flow rate, '$(u_j S_j)|_{\text{C}}$'. To avoid odd–even decoupling of the pressure field due to the co-located grid, a variation of the pressure adjusted interpolation originally proposed by Rhie and Chow [10] is employed in the present work.

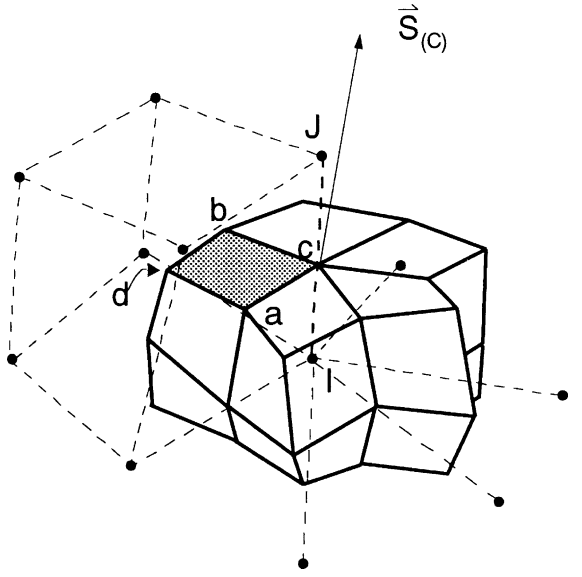

Fig. 2. Three-dimensional median-dual control volume for a typical grid point 'I' ('c' is the mid-point of the line I–J; 'a' and 'b' are face centers and 'd' is the center of the hexahedron).

3.3. Treatment of diffusion terms

The diffusion terms appearing in Eq. (4) are approximated using Eq. (8).

$$\int\int_{\text{Surf}} \left(\Gamma \frac{\partial \phi}{\partial x_j} n_j \right) \mathrm{d}s \approx \sum_{\text{NIneighbors}} \Gamma|_{\text{C}} \left.\frac{\partial \phi}{\partial x_j}\right|_{\text{C}} S_j|_{\text{C}} \tag{8}$$

In Eq. (8) a linear interpolation is used for '$\Gamma|_{\text{c}}$' and the gradient of ϕ is determined using Eq. (9).

$$\left.\frac{\partial \phi}{\partial x_i}\right|_{\text{C}} \approx \frac{\phi|_{\text{J}} - \phi|_{\text{I}}}{\Delta_{(\text{IJ})}} B_i + \frac{1}{2} \left(\left.\frac{\partial \phi}{\partial x_i}\right|_{\text{I}} + \left.\frac{\partial \phi}{\partial x_i}\right|_{\text{J}} \right) - \frac{1}{2} \left(\left.\frac{\partial \phi}{\partial x_j}\right|_{\text{I}} + \left.\frac{\partial \phi}{\partial x_j}\right|_{\text{J}} \right) B_j B_i \tag{9}$$

3.4. Pressure and velocity coupling

To couple the momentum and continuity equations, the pressure algorithm, SIMPLE [11], is adapted for the co-located grid and whole system is solved iteratively.

4. Computational domain, grids and boundary conditions

Fig. 3 gives the details of the computational domain and Table 1 the geometry and flow conditions for the base case in this study. As can be seen in Table 1, the domain extends one diameter upstream of the baffle plate where uniform velocity profiles are assumed. Non-slip boundary condition is applied to all walls and surfaces of the baffle plate. A zero normal gradient boundary condition is assumed at the exit which from Table 1 is located 15 diameters downstream of the baffle plate.

Reynolds number, Re_D is based on the can diameter and the mean velocity over the cross-sectional area of the can. It should be emphasized that all cases considered have the same mass ratio of fuel and oxidizer streams so that comparisons of the mixing fields show directly the performance of the baffle plate design. The value of $m_1/m_2 = 0.0488$ was chosen to approximately correspond to a methane/air combustor operating with about 18% excess air.

The computational grid for the base case is shown in Fig. 4. As can be seen, the flexibility of the unstructured method allows very accurate representation of the complex geometry. The adopted computational domain includes the whole of the full 360° in the peripheral direction. This provides a check on the symmetry and allows for the possibility that the flow may become asymmetrically unsteady. Control volumes are allocated finely on the edges of the jets and in the close vicinity of the baffle plate. Using finer grid spacing than that shown in Fig. 4 was found to produce little change to predicted flow and mixing patterns indicating low grid dependency for the cases considered in the present study.

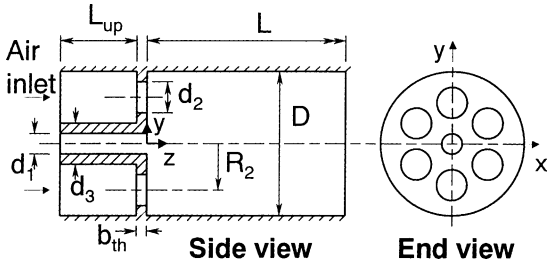

Fig. 3. Details of computational domain and location of Cartesian frame of reference.

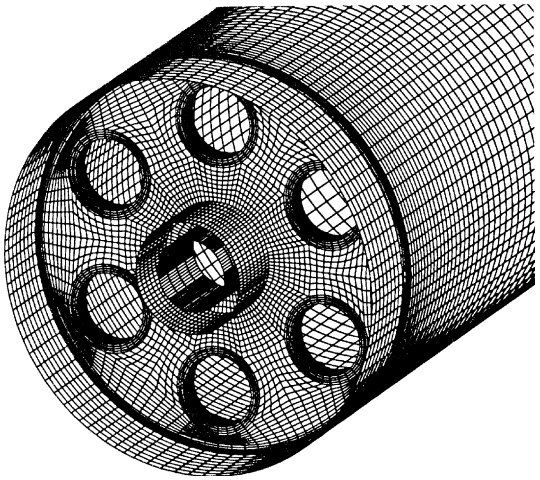

Fig. 4. Computational grid on the boundary of the domain from the upstream side of the baffle plate (base case).

5. Overall effect of baffle plate

To assess the overall performance of the design, it is useful to compare the present geometry with the much simpler co-axial jet case where no baffle plate is used. Fig. 5a and b show the mixture fraction distribution for these two cases where $Re_D = 100$ (cf. Table 1). In Fig. 5a it is apparent that the downstream end of the mixture fraction iso-surface $\xi = 0.055$ is less than one can diameter from the baffle plate. This is a remarkable improvement on the co-axial jet case where the tip of this surface is over four diameters downstream of the inlet for the same flow rates of fuel and oxidizer.

The reason for this dramatic improvement to the mixing performance can be established by examining the flow fields for the two cases. Fig. 6 gives three-dimensional representations of the flow fields together with the mixture fraction iso-surfaces for the cases shown in Fig. 5a and b. Outer surfaces of the cylindrical sections given in Fig. 6 show the results at $r/D = 0.47$ and the front surface illustrates a slice of the domain at a position just downstream of the baffle plate where $z/D = 0.15$.

Fig. 6a shows the very complex nature of the flow field in the baffle plate case. A large region of reverse flow appears in the center of the can in front of the fuel jet. This produces a stagnation point immediately in front of the fuel inlet and forces the fuel stream to flow outwards in the positive radial direction. In particular it is apparent that the fuel stream flows into the regions

Table 1
Flow conditions and geometry of computational domain for base case

d_1/D	d_2/D	R_2/D	b_{th}/D	d_3/D	L/D	L_{up}/D	Re_D	m_1/m_2	Inlet-profiles
0.182	0.182	0.341	0.05	0.282	15	1	100	0.0488	Flat

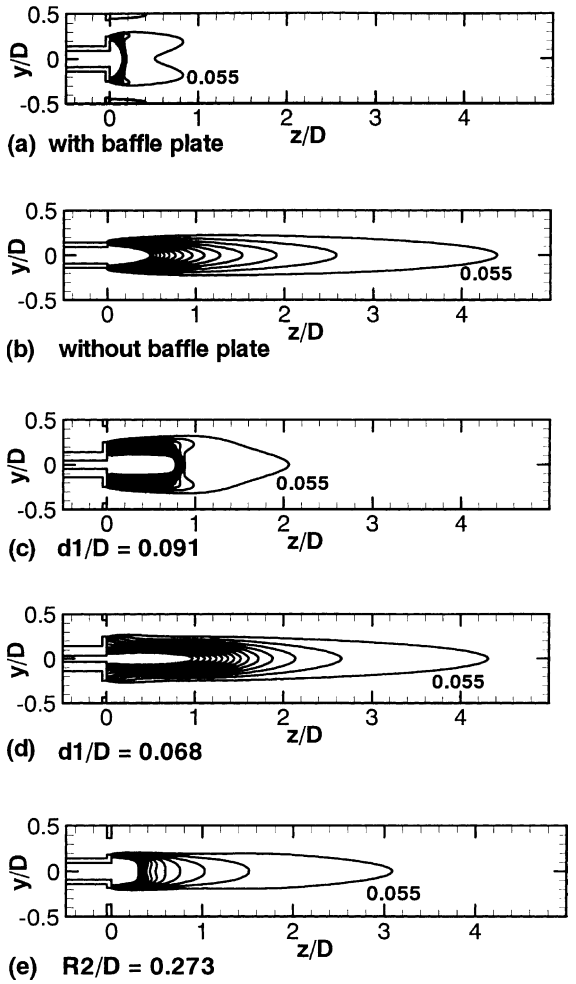

Fig. 5. Mixture fraction distributions for various configurations of the baffle plate ($x = 0$ plane).

between neighboring oxidizer jets. The complex flow structure promotes rapid mixing as can be seen by the close proximity of the mixture fraction contours to the combustion chamber inlet. In contrast, the flow field for the co-axial case in Fig. 6b is relatively simple with no recirculation and very little change in the radial components of the velocity vectors. Thus in the co-axial case, mixing of fuel and oxidizer streams is dominated by the time scale for molecular diffusion with little enhancement due to the convective field.

6. Effect of fuel jet diameter

From a close examination of Fig. 6 one might expect that if the velocity of the fuel stream is increased, the region of reverse flow in the center of the can may become less dominant and thus alter the convective enhancement to the mixing process. To examine this possibility and yet maintain the same flow rate of fuel and oxidizer, we have reduced the diameter of the fuel jet whilst keeping all other parameters constant. Fig. 5a, c and d show calculated mixture fraction fields for three different diameters of the fuel tube. Clearly, as the diameter is decreased, the enhancement to mixing is diminished. In fact in the case of a very small diameter, Fig. 5d, the overall mixing pattern is not much of an improvement on the co-axial jet case shown in Fig. 5b.

Fig. 7 gives velocity vectors for the three different fuel jet diameters. The solid lines in Fig. 7 represent the mixture fraction surface $\xi = 0.055$. In Fig. 7a (the base case) the flow field is highly recirculating with a large region of reverse flow in the center of the can as mentioned above. The stagnation point in front of the fuel jet moves further downstream in Fig. 7b and the velocity of the reverse flow diminishes. In Fig. 7c the stagnation point has disappeared altogether. There is still some reverse flow between the jets in Fig. 7c in order to satisfy the entrainment appetite of the jets. However this minor recirculation appears to do little towards enhancing the mixing as is evident in Fig. 5d. The ratios of fuel velocity to mean oxidizer velocity through the holes are 0.293,

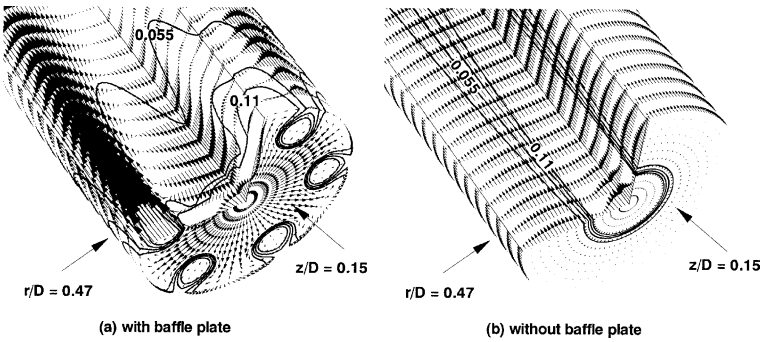

Fig. 6. Overall performance of baffle plate. Velocity vectors and mixture fraction contours.

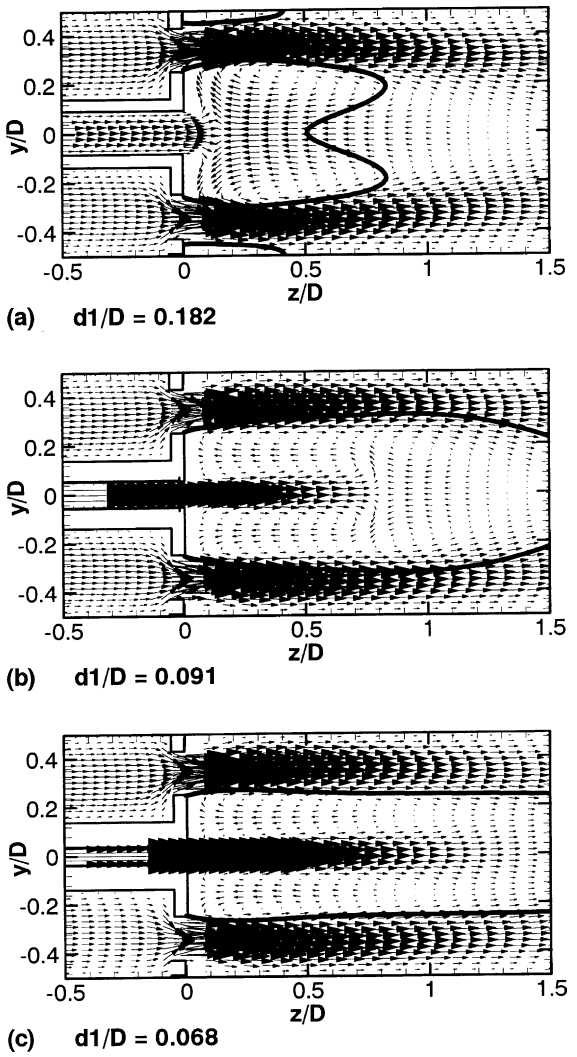

Fig. 7. Velocity vectors for different fuel jet diameters ($x = 0$ plane). The solid line represents the mixture fraction iso-surface $\xi = 0.055$.

1.17 and 2.08 for Fig. 7a, b and c, respectively. Hence we can observe that the stagnation point in front of the fuel jet moves further downstream as the fuel velocity approaches the oxidizer jet velocity and this point disappears for the case where the fuel velocity has exceeded twice the oxidizer jet velocity.

From Figs. 7 and 5a, c and d we can conclude two things. Firstly, in terms of mixing enhancement it is valuable to have a low velocity fuel jet in comparison to the oxidizer jet velocity. Hence it is desirable to have a large diameter fuel injection tube at the inlet to the combustor. Secondly, the stagnation point and strong recirculation region in the center of the can shown in Fig. 7a are valuable flow features for convective mixing enhancement.

7. Effect of oxidizer hole diameter

Having considered the effect of the fuel jet diameter, an alternative method for adjusting the velocity ratio of fuel and oxidizer streams is to change the diameters of the holes in the baffle plate for the same total flow rate and a fixed fuel jet diameter. Fig. 8 shows the resulting flow and mixing patterns for both larger (a) and smaller (b) hole diameters. For the larger hole diameter, the velocity through the holes is greatly reduced and so is the reverse-flow velocity in the center of the can. The extent of the recirculation region also is reduced significantly in comparison with Fig. 7a. The stagnation point in front of the fuel jet is a little further downstream in Fig. 8a relative to the base case, but not as far downstream as that in Fig. 7b. This might be expected as the velocity ratio of fuel to oxidizer jets is 0.46 in Fig. 8a which is greater than that for Fig. 7a (0.29) but less than that for Fig. 7b (1.17).

Conversely, reducing the oxidizer hole diameters produces an increase in the velocities and an expansion of the reverse-flow region as shown in Fig. 8b. The mixture fraction contour in Fig. 8b comes to an almost rectangular shape at $z/D = 0.15$ just in front of the fuel jet indicating very abrupt changes in gas composition. In comparison with Fig. 7a, it appears that more fuel has been forced out into the region between the oxidizer jets

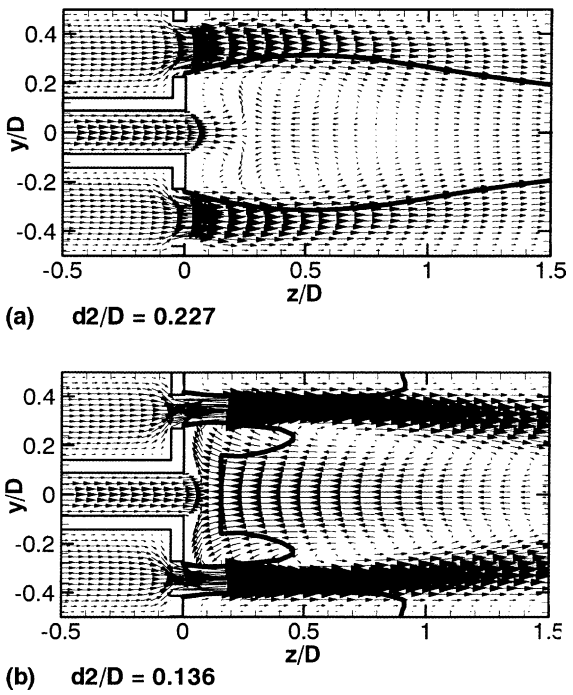

Fig. 8. Effect of: (a) enlarging and (b) reducing the oxidizer hole diameters whilst maintaining the same total flow rates of fuel and oxidizer ($x = 0$ plane). The solid line represents the mixture fraction contour $\xi = 0.055$.

and the wall of the combustor. This is apparent as the mixture fraction contour at the wall extends to about $z/D = 0.9$ in Fig. 8b and to $z/D = 0.4$ in Fig. 7a. The tendency in Fig. 8b to push too much fuel into the near-wall region indicates that for rapid mixing there is an optimum velocity ratio for the fuel and oxidizer streams. We may expect from the cases considered in this present work that this ratio will fall between cases (b) 0.165 and (a) 0.457 in Fig. 8 and is probably close to that of the base case (Fig. 7a). In summary, the overall mixing performance appears to be similar or slightly better in the base case (Fig. 7a) than in either of the cases shown in Fig. 8.

8. Effect of oxidizer hole radial position

A further parameter that requires examination is the effect of the radial location of the holes in the plate. Fig. 5e shows the effect on the mixing field of moving the holes a little closer to the center. Again this relatively small change in the geometry produces a surprisingly large change in the mixing pattern.

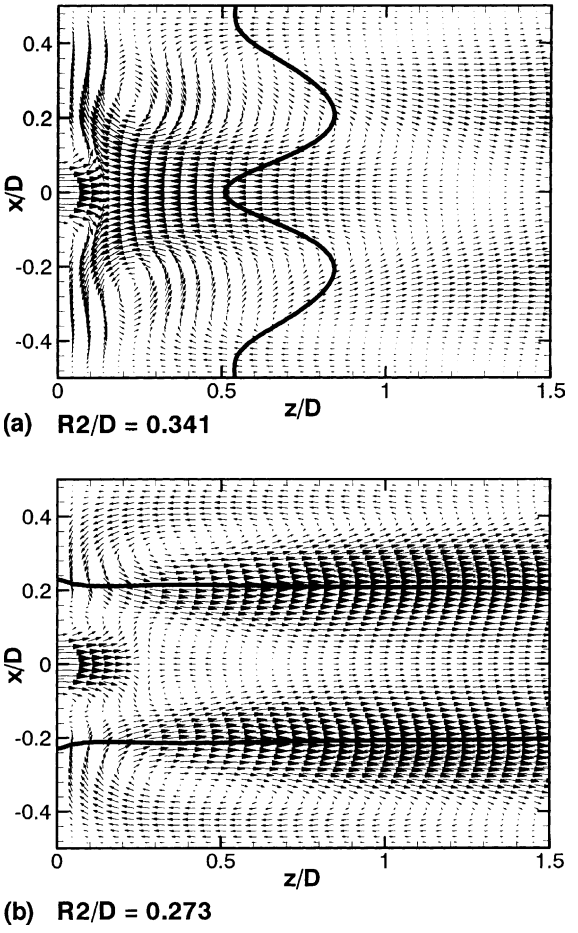

Fig. 9. Flow and mixing patterns for different radial positions of holes ($y = 0$ plane). The solid line represents the mixture fraction contour $\xi = 0.055$.

The reason for the vast difference between cases (a) and (e) in Fig. 5 again can be established through an examination of the flow fields. Fig. 9 shows velocity vectors in a plane cut between neighboring oxidizer jets. The flow structure for the two cases is considerably different. In Fig. 9a, which shows the base case, there is a very large region of reverse flow in the center of the can compared with the tiny region appearing at about $z/D = 0.5$ in Fig. 9b. The fact that neighboring jets are closer together in case b is evidenced by the much higher velocities in the regions around $x/D = \pm 0.2$ from $z/D = 0.5$ to 1.5. Also there is a pair of counter rotating recirculation regions having eyes positioned 0.2 diameters downstream of the baffle plate and at $x/D = \pm 0.3$ in Fig. 9a. In Fig. 9b these structures are not present and a pair of recirculating structures that are rotating in the opposite direction appear near the combustion chamber wall. As a result of this difference we can see in Fig. 9a the fuel stream flows directly into the region between the oxidizer jets whereas in Fig. 9b the velocity in this region is in the negative radial direction, thus inhibiting the convective enhancement to mixing. As an overall observation from Fig. 9 we can conclude that the entrainment appetite of the oxidizer jets is satisfied largely from fuel rich fluid in the center of the can in Fig. 9a but from leaner fluid in the region nearer the wall in Fig. 9b. Thus it is advantageous to place the holes in the baffle plate nearer the wall for mixing enhancement in the laminar regime.

9. Effect of Reynolds number

As one may wish to operate the combustor for a range of flow rates with a similar fuel/oxidizer ratio, it is constructive to consider the effects of Reynolds number based on the diameter of the can and the mean velocity over the full cross-sectional area of the can.

Many laminar flow fields such as sudden expansion duct flow [12], backward facing step flow [13] and laminar free jets [14] expand almost linearly in the streamwise direction in proportion to an increase in Reynolds number. The same is found true for laminar confined coaxial jets as can be seen by comparing the mixture fraction fields shown in Figs. 10a, b and 5b. Thus generally the laminar mixing problem also increases in proportion to Reynolds number until a transition to unsteady or turbulent flow is achieved.

Fig. 10c and d show the mixture fraction fields for the baffle plate case for an increase from $Re = 50$ to 200 whilst maintaining a fixed fuel/oxidizer ratio. For both cases the mixing is greatly enhanced in comparison with

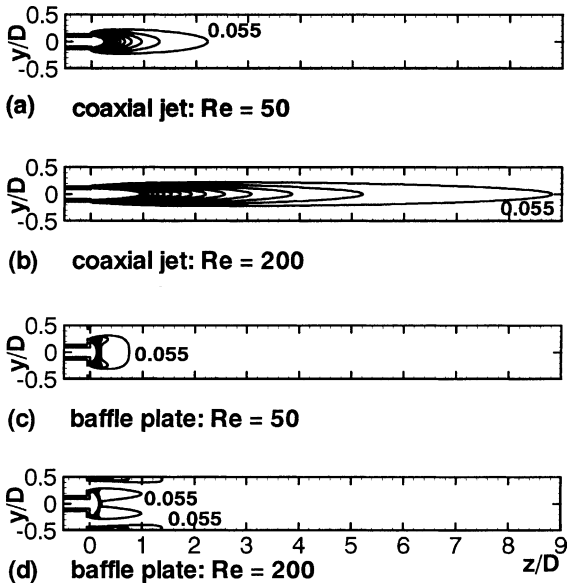

Fig. 10. Effect of Reynolds number—Mixture fraction fields ($x = 0$ plane)

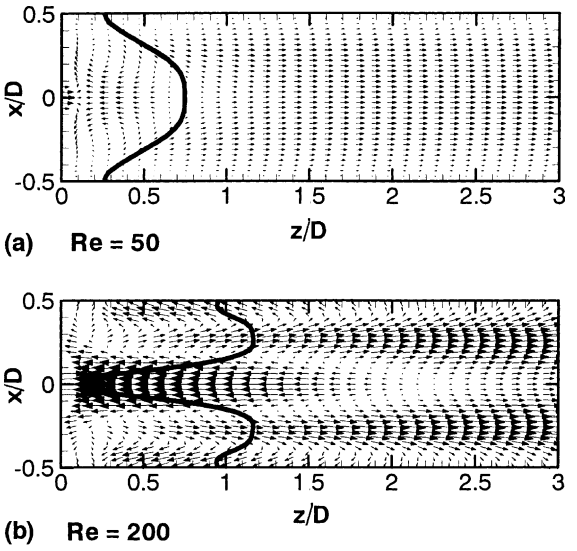

Fig. 11. Effect of Reynolds number based on the can diameter and mean velocity over cross-section; ($y = 0$ plane). The solid line represents the mixture fraction contour $\xi = 0.055$.

the cases without the baffle plate shown in Fig. 10a and b. Clearly from Fig. 10, while the mixing field expands linearly with Reynolds number in the axial direction for the co-axial jet cases, the same is not true for the baffle plate cases.

Fig. 11 shows the flow and mixing patterns for the present geometry at Reynolds numbers of 50 and 200 in the $x = 0$ plane. Comparing Fig. 11a with Fig. 11b, increasing Reynolds number from 50 to 200 does in fact produce a general expansion of the flow field in the axial direction. However, in contrast to the co-axial jet case, not all features expand directly in proportion to *Re* over this range. In particular, the stagnation point in front of the fuel jet is located at a similar axial position for $Re = 50$ (Fig. 11a), $Re = 100$ (Fig. 9a) and $Re = 200$ (Fig. 11b). Also, the mixture fraction contour $\xi = 0.055$ at the center of the can moves closer to the baffle plate as Reynolds number is increased. On the other hand, the downstream stagnation point at around $z/D = 1.25$ in Fig. 9a appears at $z/D = 0.7$ in Fig. 11a and at $z/D = 2.3$ in Fig. 11b. Also the point where the mixture fraction contour $\xi = 0.055$ touches the wall moves up or downstream roughly in proportion to Reynolds number comparing Fig. 11a and b with Fig. 9a.

The differences between the co-axial case and the baffle plate case can be explained by a consideration of the meaning of Reynolds number. Reynolds number gives a measure of the importance of convection or inertial terms with respect to diffusion terms. In the case of the co-axial jet, cross-stream transport is dominated by diffusion and stream-wise transport by convection. Thus Reynolds number for the co-axial jet case gives a measure of the ratio of stream-wise transport with respect to cross-stream transport. In such a case it is easy to see that an increase in Reynolds number will produce a corresponding increase in the length of the flow field in the stream-wise direction. In the baffle plate case however, particularly in the vicinity of the stagnation point and near the tight recirculation zones, transport in the radial direction is clearly a combination of both convection and diffusion. Moreover, due to the steep gradients appearing in the axial direction, transport by diffusion in the axial direction will also play a role. Thus Reynolds number is no longer a clear cut measure of the ratio of axial transport with respect to radial transport and the proportional expansion of the flow field with *Re* is not so obviously apparent in the baffle plate case. As a result, the mixing performance of the present design is less sensitive to an increase in *Re* from 50 to 200 than what is observed of the corresponding co-axial jet case.

10. Conclusions and closing remarks

The main findings and conclusions of this present work on the chosen geometry with isothermal, constant density flow can be summarized as follows.

1. The baffle plate can produce a dramatic improvement to mixing when compared with the co-axial jet case.
2. Relatively small changes in the geometry of the baffle plate can have a major effect on the mixing performance of the design for laminar jets.

3. To promote mixing it is desirable to reduce the velocity of the fuel stream by enlarging the diameter of the fuel jet or increase the oxidizer jet velocity by decreasing the diameters of the holes in the baffle plate.
4. The velocity ratio of fuel and oxidizer streams at the baffle plate appears to be an important consideration in characterizing the flow field.
5. To promote convective enhancement of mixing for the laminar conditions considered, it is advantageous to place the holes in the baffle plate nearer the wall of the combustion chamber.
6. For the range of Reynolds number from 50 to 200, the multi-hole baffle plate design was found less sensitive to an increase in *Re* than a confined co-axial jet with the same flow ratio of fuel and oxidizer.

Acknowledgements

This work was supported through the project "Micro Gas Turbine/Fuel Cell Hybrid-Type Distributed Energy System" by the Japan Science and Technology Corporation (JST) as Core Research of Evolutional Science and Technology (CREST). The support of the Japan Society for the Promotion of Science (JSPS) for the first author also is gratefully acknowledged.

References

[1] K. Suzuki, J.H. Kim, K. Teshima, Solid oxide fuel cell and micro gas turbine hybrid cycle for a distributed energy generation system, Key-note, in: Proceedings of the Fourth KSME-JSME Thermal Engineering Conference 3, Kobe, Japan, 2000, pp. 1–7.

[2] I.A. Waitz, G. Gauba, Y. Tzeng, Combustors for micro-gas turbine engines, Trans. ASME, J. Fluids Eng. 120 (1998) 109–117.

[3] P.L. Woodfield, K. Nakabe, K. Suzuki, The effect of three-dimensional recirculation flow structures on flow mixing of micro-scaled confined jets, in: Proceedings of the 13th International Symposium Transport Phenomena, Elsevier, Victoria, Canada, 2002, pp. 381–386.

[4] T.A. Ameel, R.O. Warrington, R.S. Wegeng, M.K. Drost, Miniaturization technologies applied to energy systems, Energy Convers. Manage. 38 (1997) 969–982.

[5] P.L. Woodfield, K. Nakabe, K. Suzuki, Performance of a three-dimensional pressure-based unstructured finite-volume method for low Reynolds number flow and wall heat transfer rate prediction, Numer. Heat Transfer, Part B, in press.

[6] D.K. Milojevic, W. Schneider, Free and confined jets at low Reynolds numbers, Fluid Dynam. Res. 12 (1993) 307–322.

[7] S.M. Hosseinalipour, A.S. Mujumdar, Flow and thermal characteristics of steady two dimensional confined laminar opposing jets: Part 1. Equal jets, Int. Commun. Heat Mass Transfer 24 (1) (1997) 27–38.

[8] D.A. Johnson, Experimental and numerical examination of confined laminar opposed jets, Part 1: Momentum imbalance, Int. Commun. Heat Mass Transfer 27 (4) (2000) 443–454.

[9] P.H. Gaskell, A.K.C. Lau, Curvature-compensate convective transport: SMART, a new boundedness-preserving transport transport algorithm, Int. J. Numer. Meth. Fluids 8 (1988) 617–641.

[10] C.M. Rhie, W.L. Chow, Numerical study of the turbulent flow past an airfoil with trailing edge separation, AIAA J. 21 (11) (1983) 1525–1532.

[11] S.V. Patankar, Numerical Heat Transfer and Fluid Flow, Hemisphere Publishing Corporation, 1980.

[12] E.O. Macagno, T. Hung, Computational and experimental study of a captive annular eddy, J. Fluid Mech. 28 (1967) 43–64.

[13] B.F. Armaly, F. Durst, J.C.F. Pereira, B. Schonung, Experimental and theoretical investigation of backward-facing step flow, J. Fluid Mech. 127 (1983) 473–496.

[14] S.I. Pai, T. Hsieh, Numerical solution of laminar jet mixing with and without free stream, Appl. Sci. Res. (The Hague) 27 (1) (1972) 39–62.